Available online at www.sciencedirect.com
SCIENCE DIRECT®
International Journal of Heat and Mass Transfer 47 (2004) 4939–4952
International Journal of HEAT and MASS TRANSFER
www.elsevier.com/locate/ijhmt

An experimental and numerical study on heat transfer enhancement for gas heat exchangers fitted with porous media

Bogdan I. Pavel, Abdulmajeed A. Mohamad *

Department of Mechanical and Manufacturing Engineering, The University of Calgary, CEERE, Calgary, Alberta, Canada T2N 1N4

Received 9 February 2010; received in revised form 25 June 2010
Available online 23 August 2010

Abstract

The present experimental and numerical work investigates the effect of metallic porous materials, inserted in a pipe, on the rate of heat transfer. The pipe is subjected to a constant and uniform heat flux. The effects of porosity, porous material diameter and thermal conductivity as well as Reynolds number on the heat transfer rate and pressure drop are investigated. The results are compared with the clear flow case where no porous material was used. The results obtained lead to the conclusion that higher heat transfer rates can be achieved using porous inserts at the expense of a reasonable pressure drop. Also, it is shown that for an accurate simulation of heat transfer when a porous insert is employed its effective thermal conductivity should be carefully evaluated.

Keywords: Forced convection; Heat transfer enhancement; Porous media

1. Introduction

The employment of different types of porous materials in forced convection heat transfer has been extensively studied due to the wide range of potential engineering applications such as electronic cooling, drying processes, solid matrix heat exchangers, heat pipe, grain storage, enhanced recovery of petroleum reservoirs, etc.

Al-Nimr and Alkam [1] numerically investigated the problem of transient forced convection flow in a concentric annuli partially filled with porous substrates located either on the inner or the outer cylinder. An increase of up to 12 times in the *Nu* number was reported in comparison with the clear annuli case and the superiority in thermal performance of the case when the porous substrate was emplaced to the inner cylinder was outlined. Based on the results obtained, Alkam and Al-Nimr [2] further investigated the thermal performance of a conventional concentric tube heat exchanger by emplacing porous substrates on both sides of the inner cylinder. Numerical results obtained showed that porous substrates of optimum thicknesses yield the maximum improvement in the heat exchanger performance with moderate increase in the pumping power. Recently, Mohamad [3] numerically investigated the heat transfer augmentation for flow in a pipe or a channel partially or fully filled with porous material emplaced at the core of the channel. It was shown that partially filling the channel with porous substrates can reduce the thermal

* Corresponding author. Tel.: +1 403 220 2781; fax: +1 403 282 8406.
E-mail address: amohamad@enme.ucalgary.ca (A.A. Mohamad).

Nomenclature

c_p	specific heat of air at constant pressure
Da	Darcy number, K/r_0^2
D_0	internal diameter of the pipe, $2r_0$
F	inertia coefficient
h	local convective heat transfer coefficient
K	permeability
k	thermal conductivity
L_0	length of the heated section
$\dot{m}$	mass flow rate of fluid
Nu	local Nusselt number, hD_0/k_f
P	dimensionless pressure
p	pressure
Pr	Prandtl number, $\mu c/k_e$
q''	exterior heat flux
Re	Reynolds number, $\rho u_m D_0/\mu$
R	dimensionless radius
r	radial position measured from the centerline
r_0	internal radius of the pipe
R_p	porous material radius ratio, r_p/r_0
r_p	radius of the porous material
T	temperature
T_{in}	temperature of the air at the inlet of the heated section (10)
T_m	local mean thermodynamic temperature of the air
T_s	local temperature measured on the heated section (10)
t	time
t^*	dimensionless time
tkr	thermal conductivity ratio, k_e/k_f
U	dimensionless axial velocity
u	axial velocity
$\|u\|$	velocity magnitude, $\sqrt{u^2+v^2}$
u_{in}	axial velocity of the air at the inlet of the heated section (10)
V	dimensionless radial velocity
v	radial velocity
v_D	Darcian velocity
Z	dimensionless axial coordinate
z	axial position measured from the beginning of the heated section (10)

Greek symbols

ε	porosity
μ	dynamic viscosity of the fluid
θ	dimensionless temperature, $\frac{T-T_{in}}{q''r_0/k_e}$
ρ	fluid density

Subscripts

e	effective
f	fluid
m	mean
s	surface
sm	solid matrix

entrance length by 50% and increase the rate of heat transfer from the walls.

It is worth mentioning that the literature contains a large number of numerical investigations and a very small number of experimental studies on the use of porous materials for natural and forced flow applications. The following lines briefly present the results obtained by authors who carried out experimental tests on porous media.

Ichimiya [4] proposed a new method for evaluation of the volumetric heat transfer coefficient between the solid material and fluid in a porous medium by conducting both experimental and numerical work. Fu et al. [5] experimentally demonstrated that a channel filled with large-conductivity porous material subjected to oscillating flow is a new and effective method for cooling electronic devices. Angirasa [6] performed experiments that proved the augmentation of heat transfer by using metallic fibrous materials with two different porosities, namely 97% and 93%. The experiments were carried out for different Reynolds numbers (17,000–29,000) and power inputs (3.7 and 9.2 W) and showed an increase in the value of the Nusselt number of about 3–6 times in comparison with the case when no porous material was used.

The present experimental and numerical study investigates the increase in the heat transfer rate between a pipe heated with a constant uniform heat flux and the air flowing inside it when different porous media are emplaced in the core of the pipe. It is shown that the accuracy of the numerical predictions depends on the prior determination of different characteristics specific to a porous material: permeability, inertia coefficient, and effective thermal conductivity. Moreover, it is shown that an objective evaluation of the real phenomena and the ones numerically simulated can help in the interpretation of the error between the numerical predictions and experimental results.

2. Problem definition

The schematic diagram of the problem is presented in Fig. 1. Flow in a pipe, partially or fully filled with porous material and heated from the exterior with a constant and uniform heat flux, is considered for both

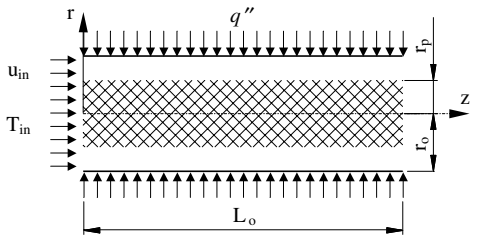

Fig. 1. Schematic diagram of the problem.

numerical and experimental investigation. In the numerical study, where the flow is assumed to be laminar, a stream of air with uniform velocity and temperature is considered to enter the pipe. Its thermophysical properties are considered to be constant for all numerical simulations. The experimental study investigates the heat transfer enhancement over a range of *Re* numbers 1000–4500 covering laminar, transient, and the beginning of the turbulent regime.

3. Experimental setup and procedure

The porous media used for experiments were manufactured from commercial aluminum screen (wire diameter 0.8 mm, density 2770 kg/m^3, thermal conductivity 177 W/m^2 K) cut out at various diameters D_p and then inserted on steel rods (see Fig. 2). That is, 12 different porous media, whose properties are presented in Table 1, were obtained by varying the screen diameter and the distance between two adjacent screens L.

The schematic diagram of the experimental facility is depicted in Fig. 3. Tests were carried out using a rig composed of four copper pipe sections ($r_0 = 31.75$ mm), joint together by flanges and screws. The last section (10) was heated at the exterior over its entire length with a uniform heat flux generated by a flexible Kapton heater (33.4 Ω), and thermally insulated from the developing region (9) with Teflon gaskets and from the environment with three layers of fiber glass with a total thickness of about 5 cm. The magnitude of the heat flux was adjusted by varying the intensity of the current measured with the ammeter (14) and supplied by the direct current power supply (6). A honeycomb rectifier of 50 mm length installed at the entrance of section (8), followed by three screens, 10 mm apart from one another, were employed in order to remove eddies and provide a more uniform velocity profile. The pressure drop caused by inserting different porous media inside the heated section (10) was measured by connecting one of the ports of the differential pressure transmitter (11) to a pressure tap, welded in the proximity of the flanges between section (9) and (10), and leaving the other one free to the atmosphere. Temperatures of the air entering the heated section and those of the surface of (10), at five axial positions (0, 49.4, 98.8, 148.2, and 247 mm) were recorded using six K-type thermocouples. The mass flow rate of air flowing inside the rig, adjusted with the help of valves (2) and pressure regulator (3), was measured using the gas flow meter (5), protected by the 50 μ-filter (4). Electrical signals generated by the sensors were transmitted to the signal conditioning unit, where they were selectively processed (the following operations were performed on the signals generated by the thermocouples:

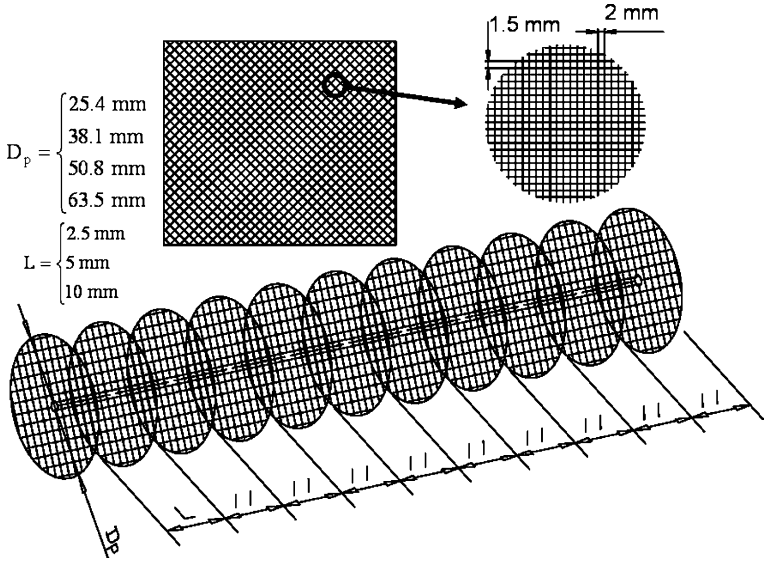

Fig. 2. Porous medium manufactured from aluminum screens.

Table 1
Porous medium characteristics

Porous medium	D (mm)	L (mm)	R_p	ε (%)	K (m^2)	F	Da
1	25.4	10	0.4	97.9 (large)	–	–	–
2	25.4	5	0.4	97.4 (medium)	–	–	–
3	25.4	2.5	0.4	96.6 (small)	–	–	–
4	38.1	10	0.6	98.8 (large)	9.409×10^{-7}	0.038	9.3341×10^{-4}
5	38.1	5	0.6	98.3 (medium)	5.947×10^{-7}	0.055	5.8897×10^{-4}
6	38.1	2.5	0.6	97.5 (small)	2.792×10^{-7}	0.069	2.7669×10^{-4}
7	50.8	10	0.8	99.1 (large)	–	–	–
8	50.8	5	0.8	98.6 (medium)	–	–	–
9	50.8	2.5	0.8	97.8 (small)	–	–	–
10	63.5	10	1.0	99.3 (large)	6.228×10^{-7}	0.032	6.1786×10^{-4}
11	63.5	5	1.0	98.8 (medium)	3.704×10^{-7}	0.046	3.6741×10^{-4}
12	63.5	2.5	1.0	98.1 (small)	1.954×10^{-7}	0.058	1.9384×10^{-4}

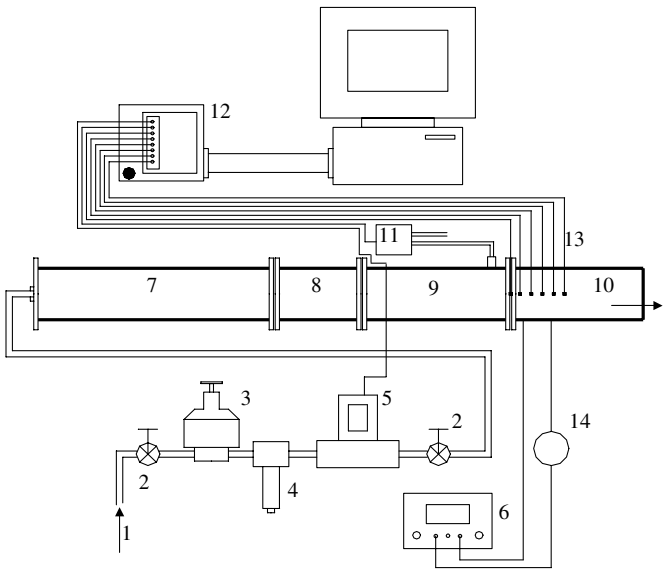

1. Compressed air
2. Valve
3. Pressure regulator
4. Filter
5. Gas flow meter
6. DC Power supply
7. Settling region (760 mm)
8. Straightener (120 mm)
9. Developing region (260 mm)
10. Heated section (500 mm)
11. Differential pressure transmitter
12. Signal conditioning unit
13. Thermocouples
14. Ammeter

Fig. 3. Experimental setup.

linearization, cold junction compensation, amplification). The resulting analog signals were further converted into digital signals by a DAQ card installed into a PC and recorded with an application developed in LabView. The characteristics and accuracy of instruments used for experiments are summarized in Table 2.

Tests were carried out for all porous media manufactured, at different mass flow rates of air and for the same power input 13.26 W. The procedure followed during each experiment is as follows. A constant power input was supplied and the mass flow rate was adjusted so that the initial value of the *Re* number was around 1000. The temperature of the air at the inlet, the temperatures on the pipe surface along the heated section, the mass flow rate of air as well as the pressure drop were continuously monitored, with a scanning frequency of 1200 Hz. Usually an initial period of approximately 3–4 h was required before reaching steady-state conditions (consid-

Table 2
Instrumentation and software used for data acquisition

	Characteristics	Manufacturer
FMA-1600 mass flow meter	Accuracy: ±1%	Omega
SCXI-1000 chassis	–	National Instruments
SCXI-1328 high accuracy isothermal terminal block	Accuracy: ±0.5% (15–30 °C), ±0.9% (0–5 °C) and (35–50 °C)	National Instruments
SCXI-1125 8-channel isolated analog input module	Offset error: ±1.5 mV/gain, gain error: ±0.03%	National Instruments
PX277 differential pressure transmitters with field selectable ranges	Accuracy: ±1%	Omega
SA1-K thermocouples	Accuracy: ±0.3%	Omega
LabView 6.0	–	National Instruments

ered to be attained, when the temperatures indicated by the thermocouples did not vary with more than ±0.3 °C within a period of about 2 min). To effectively remove the noise specific to each sensor as well as the noise induced in the electric wires by the surrounding electromagnetic fields, each data point was obtained by averaging 300 discrete values acquired with the above mentioned frequency of 1200 Hz. After collecting a set of data at steady-state conditions, the mass flow rate of air was increased so that the next value of the *Re* number differed from the previous one by about 250 units. A new set of data was collected when steady-state conditions were reached again, usually within a period of approximately 30 min. That is, the mass flow rate of air was increased progressively until a maximum value (limited by the source of compressed air) of $Re \sim 4500$ was reached.

Heat losses from the heated section (10) to the adjacent section (9) by conduction, to the atmosphere by radiation and natural convection were accounted for by performing separate experimental tests for each porous medium. The procedure followed in this case is as follows. Small amounts of heat were supplied to the electrical heater without having air flow inside the rig. After reaching steady-state conditions, temperatures along the heated surface were recorded and averaged. The heat input supplied to the heater was considered to be the same as the heat losses that occur during forced convection. This assumption holds as long as the temperature potential between the pipe and the ambient air, driving the above mentioned phenomena, is the same. In the present study the temperature of the compressed air was very close to the ambient temperature in the room. Hence, by doing a least-square fit, heat losses were expressed as functions of the average temperature of the heated surface. The coefficients resulted from the polynomial regression were updated in the application developed in LabView every time a new porous medium was tested and the heat losses were deducted from the heat input.

To check the repeatability of the measurements, different sets of readings were collected on different days

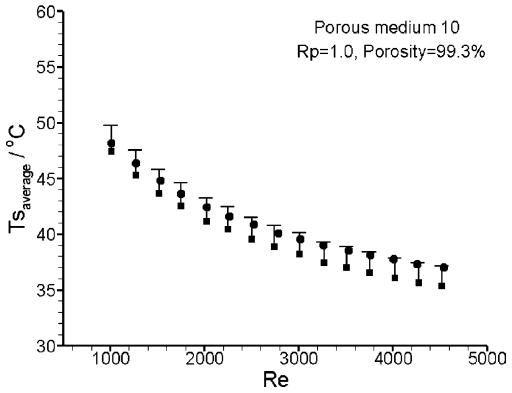

Fig. 4. Repeatability test.

using the same porous medium 10 (see Table 1). The results plotted in Fig. 4 indicate that the maximum deviation between the two sets of data is less than 5%.

The porosity of each porous medium (see Table 1) was determined by measuring the mass of all screens present in its structure.

In order to compare the numerical predictions with the experimental results, permeability K and inertia coefficient F of six of the porous media were experimentally determined by using the Forcheimer equation:

$$\Delta p = \frac{\mu L_0}{K} v_D + \frac{\rho F L_0}{\sqrt{K}} v_D^2 \tag{1}$$

Eq. (1) can be rewritten in the following form:

$$\Delta p = \alpha v_D + \beta v_D^2 \tag{2}$$

where the coefficients α and β are defined as follows:

$$\alpha = \frac{\mu}{K} L_0 \quad \text{and} \quad \beta = \frac{F}{\sqrt{K}} \rho L_0 \tag{3}$$

The procedure followed relies on measuring the pressure drop Δp over a porous medium, in a pipe of a radius equal to that of the porous material, at different Darcian velocities v_D. By fitting a second order polynomial through these points (see Fig. 5 (a) and (b)) the coefficients α and β given in Eq. (3) can be determined.

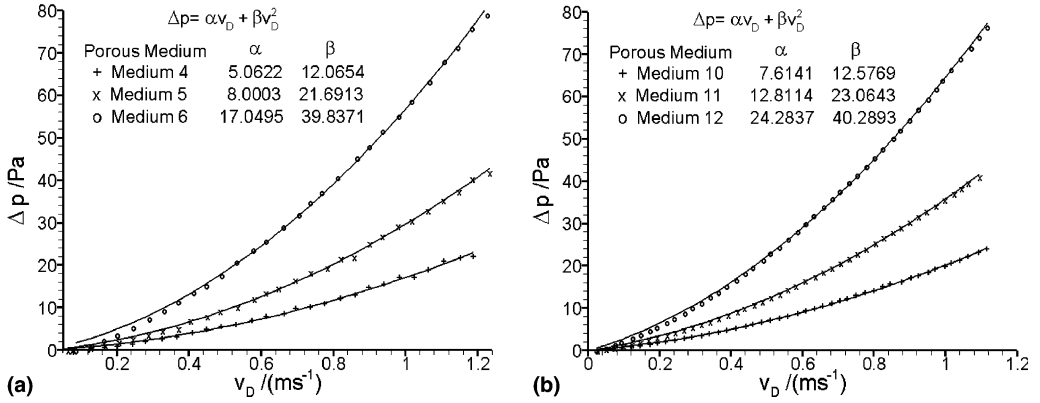

Fig. 5. Experimental determination of K and F: (a) porous mediums 4, 5, 6; (b) porous mediums 10, 11, 12.

Fig. 5 (a) and (b) present the pressure drops measured at different flow velocities over the porous media 4, 5, 6 and 10, 11, 12, respectively (see Table 1). The solid lines in these figures indicate the curves fitted through the experimental points.

By plugging the values of α and β from these figures into Eq. (3) one can obtain the corresponding values for permeability K and inertia coefficient F. Then, using the values for permeability K, one can also determine the corresponding Da numbers. The values of these parameters are summarized in Table 1.

4. Governing equations

For the numerical investigation, the system of partial differential equations governing the flow and heat transfer is given by Eqs. (4)–(7). The problem was simplified by considering the followings: the flow is assumed to be two-dimensional (symmetry about the centerline), laminar and steady; the heat generated by the viscous effects is negligible and there is no heat generation inside the pipe; the gravitational effect of the air flowing through the pipe is negligible; by writing one energy equation it was assumed that there is a local thermal equilibrium between the solid matrix and the fluid phase [3].

continuity

$$\frac{\partial}{\partial z}(\rho u)+\frac{1}{r}\frac{\partial}{\partial r}(r\rho v)=0 \tag{4}$$

z-momentum

$$\begin{aligned}&\frac{\partial}{\partial z}(\rho uu)+\frac{1}{r}\frac{\partial}{\partial r}(r\rho vu)\\&\quad=-\frac{\partial p}{\partial z}+\frac{\partial}{\partial z}\left(\mu_e\frac{\partial u}{\partial z}\right)+\frac{1}{r}\frac{\partial}{\partial r}\left(r\mu_e\frac{\partial u}{\partial r}\right)\\&\qquad-f\frac{\mu u}{K}-f\frac{\rho F}{\sqrt{K}}\mid u\mid u\end{aligned} \tag{5}$$

r-momentum

$$\begin{aligned}&\frac{\partial}{\partial z}(\rho uv)+\frac{1}{r}\frac{\partial}{\partial r}(r\rho vv)\\&\quad=-\frac{\partial p}{\partial r}+\frac{\partial}{\partial z}\left(\mu_e\frac{\partial v}{\partial z}\right)+\frac{1}{r}\frac{\partial}{\partial r}\left(r\mu_e\frac{\partial v}{\partial r}\right)\\&\qquad-f\frac{\mu v}{K}-f\frac{\rho F}{\sqrt{K}}\mid u\mid v-\frac{\mu v}{r^2}\end{aligned} \tag{6}$$

energy

$$\begin{aligned}&\frac{\partial}{\partial z}(\rho cuT)+\frac{1}{r}\frac{\partial}{\partial r}(\rho crvT)\\&\quad=\frac{\partial}{\partial z}\left(k_e\frac{\partial T}{\partial z}\right)+\frac{1}{r}\frac{\partial}{\partial r}\left(rk_e\frac{\partial T}{\partial r}\right)\end{aligned} \tag{7}$$

The parameter f is set to unity for flow in porous medium and to zero for flow in a region without porous material. The flux continuity (momentum and energy) is ensured by evaluating the harmonic mean values of the physical properties (viscosity, thermal conductivity) at the interface between the clear fluid and the fluid-saturated porous medium. In the energy equation, k_e is the effective thermal conductivity of the medium.

The boundary conditions used are as follows:

$$\begin{aligned}&\underline{r=0}:\begin{cases}\frac{\partial u}{\partial r}=0\\ v=0\\ \frac{\partial T}{\partial r}=0\end{cases}\quad \underline{r=r_0}:\begin{cases}u=0\\ v=0\\ \frac{\partial T}{\partial r}=\frac{q''}{k_f}\end{cases}\\&\underline{z=0}:\begin{cases}u=u_{in}\\ v=0\\ T=T_{in}\end{cases}\quad \underline{z=L_0}:\begin{cases}\frac{\partial u}{\partial z}=0\\ \frac{\partial v}{\partial z}=0\\ \frac{\partial T}{\partial z}=0\end{cases}\end{aligned} \tag{8}$$

The above Eqs. (4)–(7) are transformed into dimensionless forms by using the inlet velocity, heat flux, and the pipe radius as references to scale velocity components, temperature and length, respectively. The dimensionless parameters are as follows:

$$\begin{aligned}&U=\frac{u}{u_{in}};\quad V=\frac{v}{u_{in}};\quad P=\frac{p}{\rho u_{in}^2};\quad \theta=\frac{T-T_{in}}{q''r_0/k_e};\\&R=\frac{r}{r_0};\quad Z=\frac{z}{r_0};\quad t^*=\frac{u_{in}}{r_0}t\end{aligned} \tag{9}$$

The dimensionless set of equations is as follows:

$$\frac{\partial}{\partial Z}(UU)+\frac{1}{R}\frac{\partial}{\partial R}(RVU) = -\frac{\partial P}{\partial Z}+\frac{\partial}{\partial Z}\left(\frac{\partial U}{\partial Z}\right)+\frac{1}{R}\frac{\partial}{\partial R}\left(R\frac{\partial U}{\partial R}\right) - f\frac{U}{ReDa}-f\frac{F}{\sqrt{Da}}\mid U\mid U$$

$$\frac{\partial}{\partial Z}(UV)+\frac{1}{R}\frac{\partial}{\partial R}(RVV) = -\frac{\partial P}{\partial R}+\frac{\partial}{\partial Z}\left(\frac{\partial V}{\partial Z}\right)+\frac{1}{R}\frac{\partial}{\partial R}\left(R\frac{\partial V}{\partial R}\right) - f\frac{V}{ReDa}-\frac{F}{\sqrt{Da}}\mid U\mid V-\frac{V}{ReR^2}$$

$$\frac{\partial}{\partial Z}(U\theta)+\frac{1}{R}\frac{\partial}{\partial R}(RV\theta)=\frac{1}{RePr}\left[\frac{\partial^2\theta}{\partial Z^2}+\frac{1}{R}\frac{\partial}{\partial R}\left(R\frac{\partial\theta}{\partial R}\right)\right] \tag{10}$$

The local Nu number for a pipe can be calculated as follows, where $\theta_m=\int_0^1 UR\theta\,dR/\int_0^1 UR\,dR$ stands for the local mean temperature of the fluid inside the pipe.

$$Nu=\frac{2}{\theta_s-\theta_m}; \tag{11}$$

A control volume, finite difference approach is used to solve the model equations with the specified boundary conditions. The SIMPLER algorithm is employed to solve the equations in primitive variables. Central difference approximations are used to approximate the advection–diffusion terms, i.e., the scheme is second order accurate in space. The governing equations are converted into a system of algebraic equations through integration over each control volume. The algebraic equations are solved by a line-by-line iterative method, which sweeps the domain of integration along the R- and Z-axis and uses the tri-diagonal matrix inversion algorithm. Velocity components are under-relaxed by a factor of 0.7. For most calculations, 4000 iterations are sufficient to get convergent solution for a 151×81 grid, and more iterations are needed for 201×201. The criteria for convergence are to conserve mass, momentum and energy globally and locally, and to ensure convergence of pre-selected dependent variables to constant values within machine error.

The assumptions made for the experimental investigation are as follows: steady-state conditions are considered; the variation of the specific heat at constant pressure c_p of air can be neglected for the temperature range encountered; changes in the kinetic and potential energy of the fluid are negligible; energy transfer by conduction in the pipe wall is negligible.

By writing the conservation of energy for a control volume located at an axial distance z, from the inlet of the heated section (10) as it is described in [7], and using relation

$$q_s''=h(T_s-T_m) \tag{12}$$

one can obtain the value for the local convective heat transfer coefficient

$$h(z)=\frac{q''}{[T_s(z)-T_m(z)]} \tag{13}$$

The local mean thermodynamic temperature of the air was deducted from the energy balance and from here the local value for the Nusselt number:

$$T_m(z)=T_{in}+\frac{q''(\pi D_0)}{\dot{m}c_p}z \tag{14}$$

$$Nu(z)=\frac{h(z)D_0}{k_f} \tag{15}$$

5. Experimental results and discussions

The length-averaged temperature of the pipe surface, length-averaged Nusselt number, and pressure drop are presented in Fig. 6(a)–(c), respectively, for all 12 porous media tested. The length-averaged values were obtained by averaging the local values of the corresponding parameters. From Fig. 6(a) it can be seen that the average temperature of the pipe surface $Ts_{average}$ decreases with the increase in Re and with the employment of porous materials in the core of the pipe.

In Fig. 6(b), by comparing the curves corresponding to the porous media with the same R_p it can be seen that a small decrease in porosity does not influence the heat transfer rate when $R_p=0.4$ and 0.6. This is not the case for $R_p=0.8$ and 1.0 where a small decrease in porosity results in a significant increase in $Nu_{average}$. The variation in porosity for the case where $R_p=1.0$ has a much stronger influence upon $Nu_{average}$ than the other cases due to the additional heat transfer by conduction resulted from the contact between the pipe surface and the porous medium. When R_p decreases to 0.8 the increase in the value of $Nu_{average}$ with the decrease in porosity is due to a channeling effect. A decrease in porosity translates into a poorer capability of the fluid to penetrate through the porous medium; hence the fluid tends to flow in the annular channel, between the cylindrical porous medium and the interior surface of the pipe, at higher velocities due to the reduction in the cross sectional area available for fluid flow. Besides the channeling effect, which causes a flow redistribution, another important factor in enhancing heat transfer especially when $R_p<1.0$ is the radiative heat transfer occurring between the pipe surface and the porous medium emplaced in the core of the pipe.

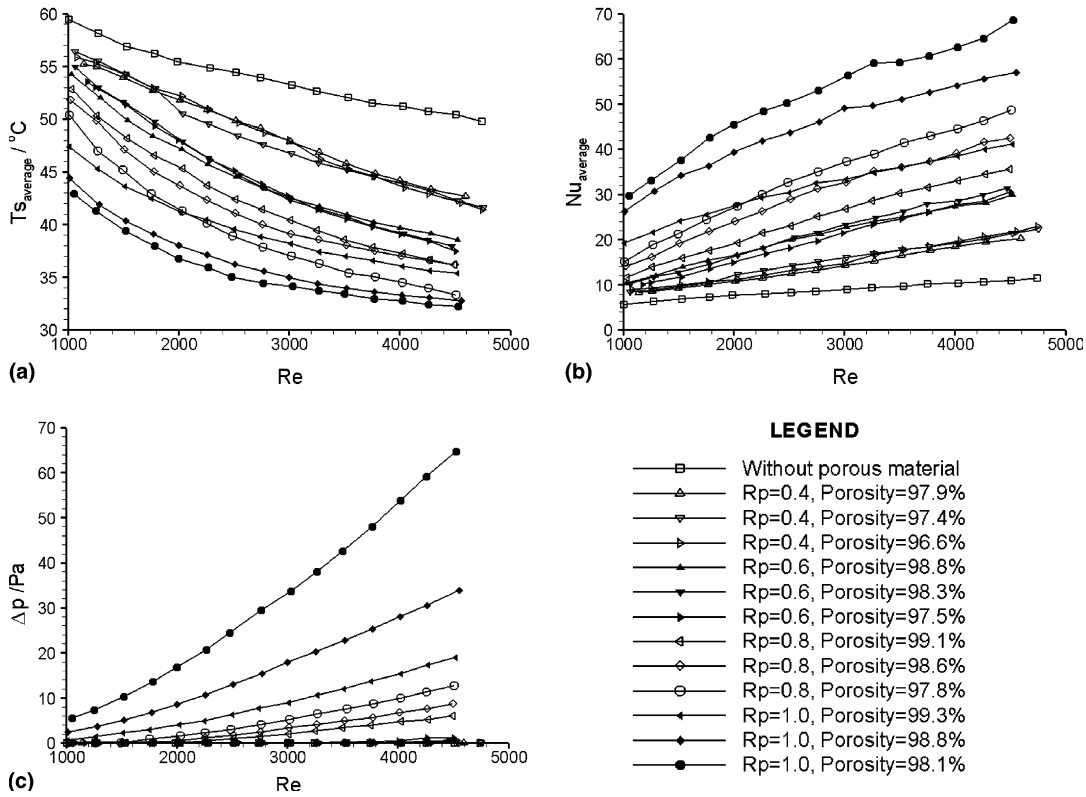

Fig. 6. Experimental results: (a) $Ts_{average}$; (b) $Nu_{average}$; (c) Δp as functions of Re.

Fig. 6(a) and (b) also illustrate the strong effect R_p has on enhancing heat transfer. By comparing the $Nu_{average}$ curves obtained with $R_p = 0.4$, 0.6, 0.8, and 1.0 with the clear flow case it can be concluded that higher heat transfer rates can be achieved by increasing R_p culminating with the case of a fully porous channel.

Heat transfer enhancement also arises from the modification of the thermal conductivity of the medium inside the pipe. For the clear flow case, the thermal conductivity of the medium inside the pipe is that of the air, which is very small, but when one of the aluminum porous media is employed the resulting effective thermal conductivity becomes much larger than that of the air.

An important factor that has to be considered when employing porous media for the purpose of enhancing heat transfer is the penalty arising from the increased pressure drop. Fig. 6(c) presents the pressure drops measured over the experimentally tested porous media at different Re. As expected, the largest pressure drops correspond to the cases that offer the best thermal performance, namely $R_p = 0.8$ and 1.0. If the pressure drops corresponding to the cases where $R_p < 0.8$ are negligible, in the other cases their values become noticeable with the decrease in porosity (for the same R_p) and with the increase in R_p.

The experimental results are summarized in Fig. 7. Fig. 7(a) presents the percentage increase in the value of the $Nu_{average}$ in comparison with the clear flow case. For each value of R_p, the minimum and maximum values correspond to the lowest and highest Re, respectively. Fig. 7(b) illustrates the pressure drops recorded for all cases, the previous observations regarding the minimum and maximum values being the same. From these figures it can be seen that the highest increase in the $Nu_{average}$ of approximately 5.28 times was obtained by fully filling the pipe at the expense of the highest pressure drop of 64.8 Pa. In comparison with fully filling the pipe, a partial filling has the advantage of a comparable increase in the Nusselt number and a smaller increase in the pressure drop.

6. Numerical results and discussions

The independent parameters whose influences on heat transfer and pressure drop are numerically analyzed can be divided in two categories: those pertaining

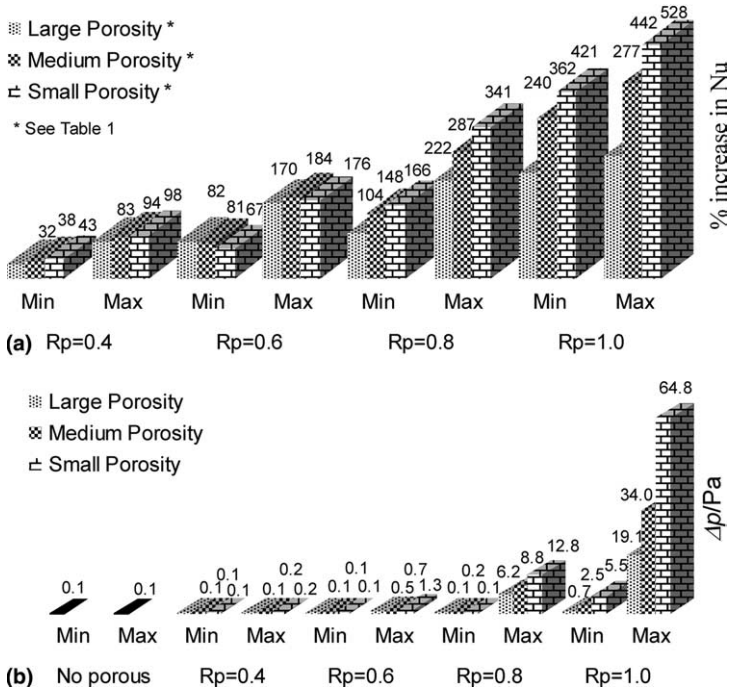

Fig. 7. Summary of the experimental results: (a) percentage increase in the value of the $Nu_{average}$ in comparison with the clear flow case; (b) the associated pressure drop.

to the porous material (*Da* number—a direct reflection of its permeability K, porous material radius ratio R_p, thermal conductivity ratio tkr, and inertia coefficient F) and the one reflecting the flow conditions (*Re*).

The large variety of porous materials makes impossible the development of a general analytical relation between the permeability of the porous material K and its inertia coefficient F. This is why, the influence of this parameter in the numerical investigation is disregarded by assuming $F = 0$.

6.1. Hydrodynamic aspects

Fig. 8(a) and (b) present the fully developed axial velocity profiles for $Da = 10^{-3}$ and 10^{-6}, respectively, and different values of R_p. From both figures it is readily seen that the increase in R_p forces the fluid to channel in the annular space created between the pipe and porous matrix. The maximum velocity of the fluid at the core of this newly formed annular channel increases and shifts toward the surface of the pipe with increasing R_p, up to $R_p = 0.8$. Moreover, as porosity decreases, the fluid velocity inside the porous medium decreases, while the velocity outside the porous region increases. That is, a larger value of R_p combined with a smaller porosity lead to higher fluid velocities located much closer to the pipe wall, consequently higher heat transfer rates. When $R_p = 1.0$ (fully filled pipe), the velocity profile becomes constant across the diameter, hence the heat transfer rate decreases.

A very important aspect, the attention should be focused on, when employing porous materials for the purpose of heat transfer enhancement is the increased pressure drop. Fig. 9(a) presents the variation of the dimensionless pressure drop versus R_p for different *Da* numbers. The pressure drop increases with the increase in R_p for a constant *Da*, and with the decrease in *Da* for a constant R_p. As the values for the pressure drop corresponding to the fully filled pipe are much larger than those corresponding to the partially filled pipe, a 0.6 or 0.8 value for R_p associated with a $Da = 10^{-4}$ or 10^{-5} would be attractive for use in enhancing heat transfer.

6.2. Thermal aspects

Fig. 10 presents the variation of the local Nusselt number for different values of $Da = 10^{-2}$, 10^{-3}, 10^{-4}, 10^{-5}, and 10^{-6}. In all cases the employment of a porous material leads to an increase in *Nu* in comparison with the clear flow case. Thermal performance for the case where $Da = 10^{-2}$ increases with the porous material diameter up to an $R_p = 0.6$ (Fig. 10(a)). Further increase in R_p up to 0.8 and even more up to 1.0 leads to a decrease in *Nu*. This is not the case when the permeability of the porous material is decreased to a corresponding

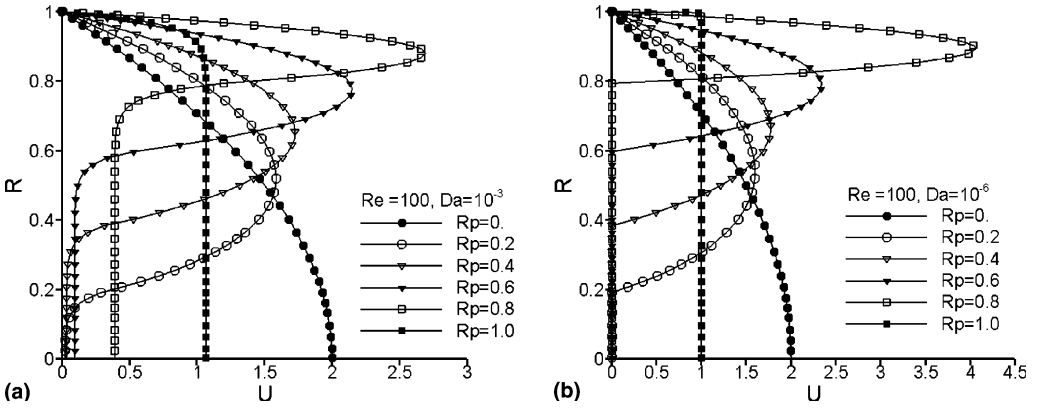

Fig. 8. Numerical predictions. Influence of R_p on the fully developed axial velocity: (a) $Da = 10^{-3}$; (b) $Da = 10^{-6}$.

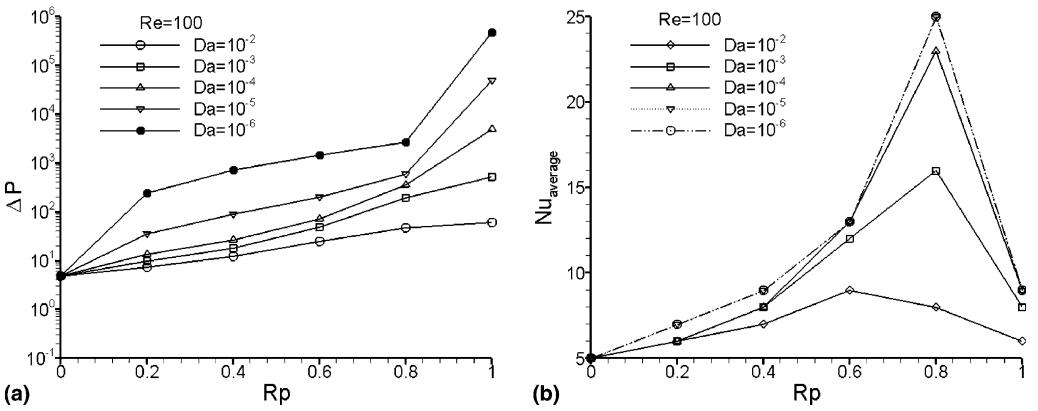

Fig. 9. Numerical predictions. Influences of R_p and Da on: (a) ΔP; (b) Nu_{average}.

$Da = 10^{-3}$ to 10^{-6} (Fig. 10(b)–(e)). In the latter cases the heat transfer increases with R_p up to 0.8, which offers a far better thermal performance than all other cases. The same effect of poorer thermal performance can be observed for these cases when R_p is increased from 0.8 to 1.0. The increase in the Nu with the increase in R_p can be attributed to the channeling effect, already described.

Fig. 9(b) presents the effect of both R_p and Da on Nu_{average}. It is interesting to notice the identical thermal performance of the cases where Da = 10^{-5} and 10^{-6}.

The influence of k_{sm} on the heat transfer rate is investigated using the dimensionless thermal conductivity ratio tkr:

$$\text{tkr} = \frac{k_e}{k_f} \tag{16}$$

For a constant thermal conductivity of the fluid k_f, tkr is a direct reflection of the effective thermal conductivity k_e. The difficulty that arises here is related to the way the effective thermal conductivity should be calculated. It is evident that it depends on the thermal conductivity of the porous matrix k_{sm}, on the thermal conductivity of the fluid k_f as well as on the structure and porosity of the porous matrix.

Fig. 11(a) presents the combined influence of R_p and Da on Nu_{average} for three different values of tkr 1, 2.4 and 10. It is clear that higher heat transfer rates can be achieved by increasing tkr, which means increasing the thermal conductivity of the solid matrix k_{sm}. An interesting observation is related to the fact that the effect of an increased k_{sm} starts being felt when $R_p = 0.8$ for large values of Da (see in Fig. 11(a) where the three surfaces starts separating) and $R_p = 0.6$ for small values of Da. This is due to the fact that heat conduction in the porous matrix plays a more significant role with decreasing permeability and increasing R_p.

As expected when the porous material is fully filling the pipe the increase in the value of k_{sm}, consequently tkr, will bring the largest increase in the heat transfer rate.

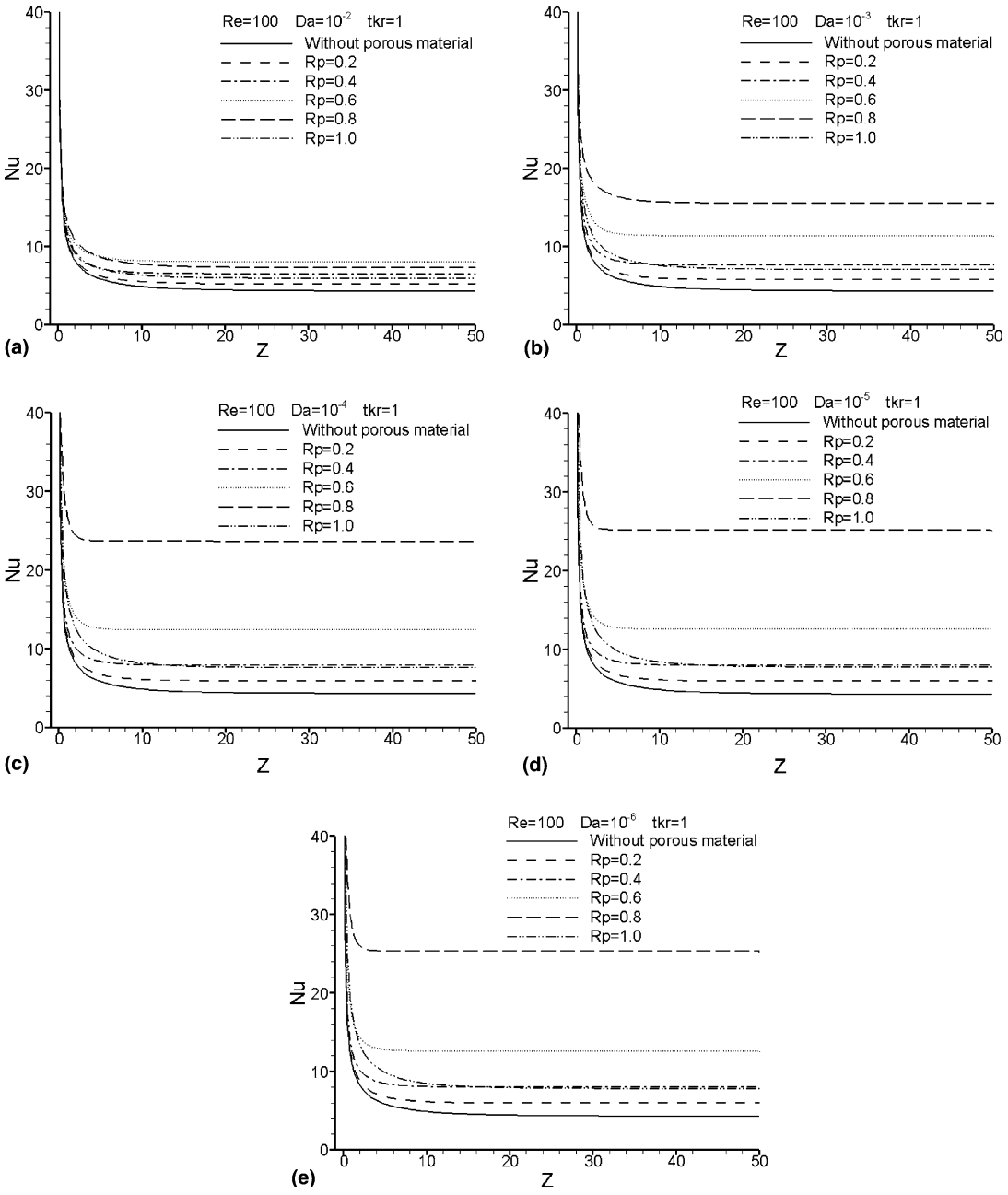

Fig. 10. Influence of R_p on local Nu: (a) $Da = 10^{-2}$; (b) $Da = 10^{-3}$; (c) $Da = 10^{-4}$; (d) $Da = 10^{-5}$; (e) $Da = 10^{-6}$.

Fig. 11(b) illustrates the combined effects of Re, R_p and Da on $Nu_{average}$. The influences of the other two parameters R_p and Da were already discussed. What should be observed, and somehow was expected, in Fig. 11(b) is the fact that a larger value of Re leads to higher heat transfer rates regardless of the values of the other two parameters R_p and Da.

7. Comparison between the numerical predictions and experimental results

The first observations that should be made are as follows: both experimental and numerical results have the same trends; the value of the Nu corresponding to the clear flow case converges to 4.36 (see Fig. 10), which is the value of Nu for thermally fully developed flow in a

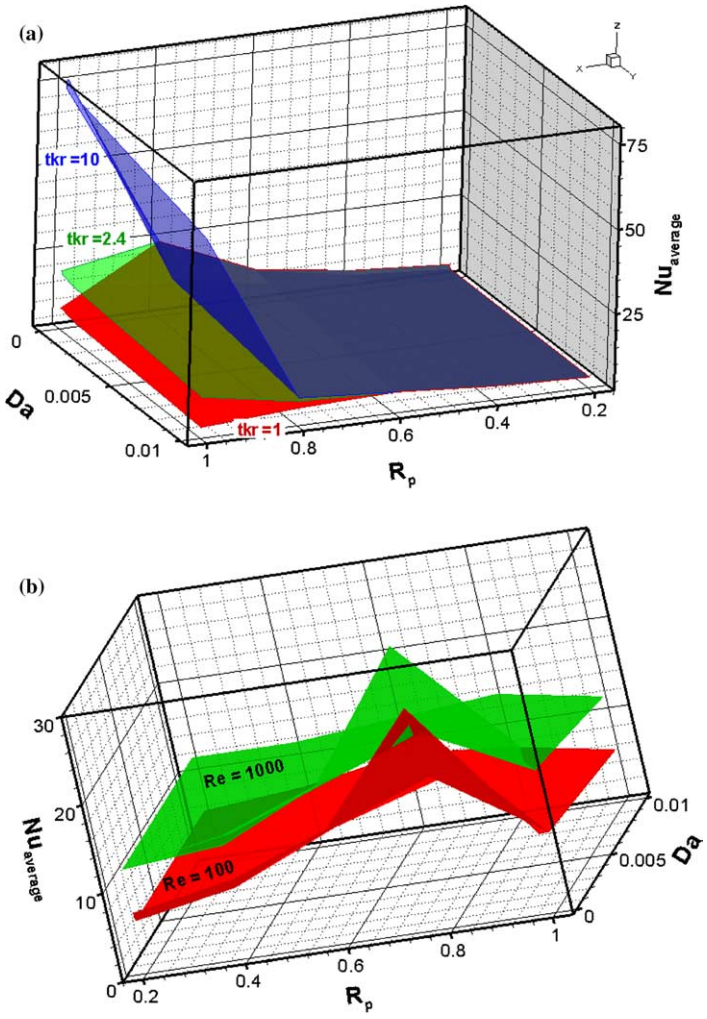

Fig. 11. Numerical predictions. Combined influences of Da, R_p and: (a) tkr; (b) Re on $Nu_{average}$.

pipe without porous material in the condition of a constant and uniform heat flux.

A direct comparison between the numerical and experimental results is difficult for the present experiment due to the following reasons:

- the numerical code is valid only for the laminar flow regime, while the experimental data is available mostly for the transient and turbulent flow regimes (Re = 1000–4500). Therefore the domain where the comparison can be carried out is restricted to a range of Re between 1000 and 2000;
- the numerical code does not simulate radiative heat transfer, while the experimental results are influenced by this mode of heat transfer. Based on this reason it is reasonable to expect the numerical results to under predict the values of Nu obtained experimentally;
- the numerical code does not account for the conductive heat transfer that takes place in the pipe wall while the experimental results are influenced by this phenomenon (conjugate effect);
- the porous media tested experimentally are homogeneous and anisotropic since they were manufactured by inserting different numbers of screens on metallic rods. On the other hand, the numerical code accounts for a homogeneous and isotropic porous medium. Motivated by this explanation one would expect the numerical results (resulted from accounting for heat conduction in the porous matrix) to over predict the values of Nu determined experimentally (no heat conduction in the porous matrix);
- there is also a contradiction between the inlet velocity profiles. The parabolic one imposed in the numerical simulation will not perfectly match the real one encountered during the experiments;

- the last motivation given here is related to the requirement of an experimental determination of the effective thermal conductivity k_e, permeability K, and inertia coefficient F pertaining to all manufactured porous media.

Out of all these problems, the last one was partially solved by determining the permeability K and inertia coefficient F for six of the manufactured porous media as it was described in Section 3.

The comparison between the numerical and experimental results will be done taking into account the observations made above and using the values presented in Table 1 as well the corresponding Re encountered experimentally. The porous media whose results are compared are 5, 6, 10, and 12 (see Table 1) covering this way the cases of partially and fully filled pipe as well as small, medium, and large values of porosity.

Fig. 12(a) and (b) reveal the difference between the experimental and numerical results corresponding to the porous media 5 and 6, respectively. The numerical results are not sensitive to the value of the thermal conductivity ratio tkr due to the large values of porosity and small value of R_p, which is in agreement with was previously shown and explained in Section 6.2 (see also Fig. 11(a)). The numerical results obtained for tkr = 1.0 are identical with those obtained for tkr = 1.5.

It is easily seen that the numerical results over predict the experimental ones and the percentage error is significant. The explanation for this fact can be reasoned based on the explanations presented earlier. For this small value of $R_p = 0.6$ and large values of permeability the over prediction of the experimental results (the numerical code simulates homogeneous and isotropic porous media) prevails over their under prediction (the numerical code does not simulate radiative heat transfer).

Fig. 12(c) and (d) reveal the difference between the experimental and numerical results corresponding to porous media 10 and 12, respectively. The numerical results for these cases are sensitive to the value of the thermal conductivity ratio tkr due to the large value of

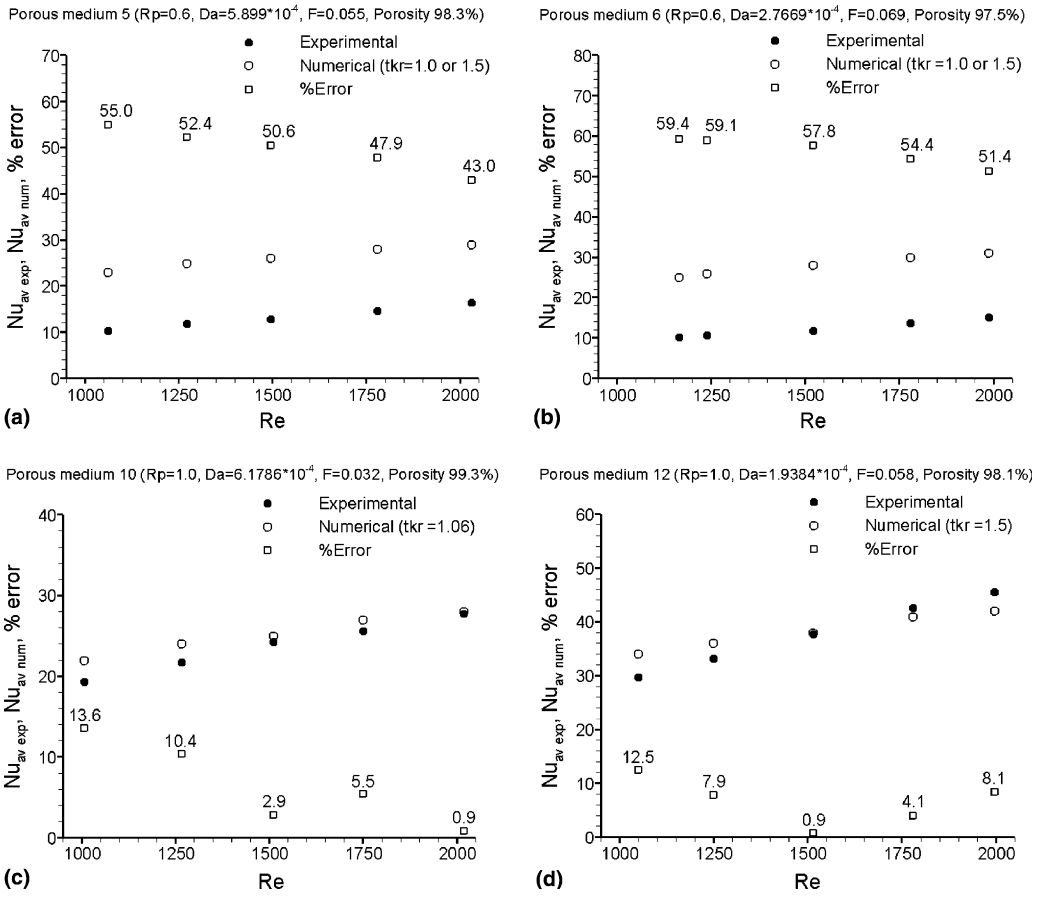

Fig. 12. Comparison between the experimental results and numerical predictions for: (a) porous medium 5; (b) porous medium 6; (c) porous medium 10; (d) porous medium 12.

$R_p = 1.0$, which again is in agreement with was shown and explained in Section 6.2. The experimental results were best matched by the numerical results when the chosen values for tkr were 1.06 and 1.5 for porous media 10 and 12, respectively. For these cases the percentage error is smaller and it seems that the two insufficiencies described earlier counterbalance each other.

In order to illustrate the discrepancies between the relations used in the literature to determine the effective thermal conductivity, k_e was calculated using two different models, namely, $k_e = \varepsilon k_f + (1-\varepsilon)k_{sm}$ and $k_e = k_f^{\varepsilon} k_{sm}^{(1-\varepsilon)}$. Thermal conductivity of air and porous media used are about 0.027 and 177 (W/m K), respectively. Hence, for $\varepsilon \approx 98\%$ the resulting values according to the above relations are 3.57 and 0.032 (W/m K), respectively. This example reveals how important it is to properly model or measure the real effective thermal conductivity, which is an input parameter for the mathematical model.

8. Conclusions

The present experimental and numerical study investigates the potential of porous inserts to enhance the rate of heat transfer occurring between the surface of a pipe heated with a constant and uniform heat flux and the air flowing inside it. The following conclusions may be drawn.

Heat transfer enhancement can be achieved using porous inserts whose diameters approach the diameter of the pipe. For a constant diameter of the porous medium, further improvement can be attained by using a porous insert with a smaller porosity and higher thermal conductivity. Care should be exercised since both R_p and ε have a positive influence upon heat transfer and a negative impact on pressure drop, consequently on the pumping power.

The main mechanisms identified to be the basis for the heat transfer enhancement when using porous materials are as follows: flow redistribution (flow channeling), thermal conductivity modification, and enhancement of the radiative heat transfer.

In conclusion it is worth emphasizing again the importance of experimental determination of the characteristics of a porous material. It is their proper determination that will ensure a successful numerical simulation.

References

[1] M.A. Al-Nimr, M.K. Alkam, Unsteady non-Darcian forced convection analysis in an annulus partially filled with a porous material, ASME J. Heat Transfer 119 (1997) 799–804.

[2] M.K. Alkam, M.A. Al-Nimr, Improving the performance of double-pipe heat exchanger by using porous substrates, Int. J. Heat Mass Transfer 42 (1999) 3609–3618.

[3] A.A. Mohamad, Heat transfer enhancements in heat exchangers fitted with porous media. Part I: constant wall temperature, Int. J. Therm. Sci. 42 (2003) 385–395.

[4] K. Ichimiya, A new method for evaluation of heat transfer between solid material and fluid in a porous medium, ASME J. Heat Transfer 121 (1999) 978–983.

[5] H.L. Fu, K.C. Leong, X.Y. Huang, C.Y. Liu, An experimental study of heat transfer of a porous channel subjected to oscillating flow, ASME J. Heat Transfer 123 (2001) 162–170.

[6] D. Angirasa, Experimental investigation of forced convection heat transfer augmentation with metallic fibrous materials, Int. J. Heat Mass Transfer 45 (2002) 919–922.

[7] F.P. Incropera, D.P. DeWitt, Introduction to Heat Transfer, 4th ed., John Wiley & Sons, New York, 2002, pp. 8.445–8.447.